CHAPTER 3

Potential Field Method

The potential field data which are gravity and aeromagnetic data are analyzed and sketchily interpretation in large scale of the study area. The objective of this chapter is to find the depth of the structure by using the radially average power spectrum method and produce the forward modeling of the gravity data. Both of potential data are used for estimate depth by radially average power spectrum method, however, the aeromagnetic are not yielded for forward modeling due to the aeromagnetic survey collected data at 762-meter height resulting the attention of magnetic values from the shallow subsurface. Moreover, the gravity survey collected data on ground survey consequently, the gravity data have been reliable for construction pseudo-geological model more than the aeromagnetic data.

The potential data which is gravity and magnetic data are suffered from the non-uniqueness because several earth models could produce the same gravity and/or magnetic response. Therefore, the forward modeling was constrained base on existed data which are seismic reflection, resistivity, and MASW data.

3.1. Potential filed data source

The nationwide aeromagnetic data of Thailand had been collected by Kenting Earth Sciences (international) Ltd. (KESIL), based in Ottawa, Canada, under the Mineral Resources Development Project (MRDP) from Department of Mineral Resources (DMR), Ministry of Industry, Thailand, during 1984-1989. Magnetic data of this study area is a part of nationwide aeromagnetic data flown in N-S direction with 1-kilometer line spacing and the sensor height 2500 feet or 762 meters mean terrain clearance. Finally, the nationwide aeromagnetic data was regrided with a grid cell size of 500 meters and at 300 meters MTC (Hatch, et al. 1994). The main geomagnetic field is removed by using the International Geomagnetic Reference Field (IGRF) during the time of observation to

obtain the residual magnetic map. The reduction to the Pole (RTP) is employed to correct asymmetric shape of magnetic anomaly due to geomagnetic field inclination (Geosoft Inc., 2007). Figure 3.1 displays the RTP of residual magnetic map from the study area with the magnetic anomaly values range from -4 to -24 nT approximately.

The gravity data were collected as ground survey under the study of geological in Northern Thailand during 2014-2015 by DMR. The ground survey covers almost the whole Northern region of Thailand. These data were collected as random points with spacing about 1 kilometer. The observed data were deducted with the conventional gravity data correction using Bouquer density of 2.67 g/cm^3 to acquire the complete Bouguer gravity map. After reduction, the gravity grid was interpolated by RANGRID algorithm with grid cell size 500 meters. Figure 3.2 is the complete Bouguer gravity map of the study area cropped from the reginal gravity map with gravity anomaly values range from -72 to -89 mGal approximately.

Figure 3.1 shows the aeromagnetic anomaly map. High magnetic anomaly zones indicated by “A” have the NE-SW trend located on northwestern part. These zones show Carboniferous sandstone, Permian limestone, and Permo-Triassic volcanic rock, and Quaternary sediment when overlaying with geological map. Intermediate magnetic anomaly zones indicated by “B” have the NE-SW trend that is located on the center of magnetic anomaly maps. These zones show Quaternary sedimentary when overlaying with geological map. The low magnetic anomaly zone indicated by “C” on is located on southeastern part of magnetic anomaly map. These zones show Carboniferous sandstone, Silurian-Devonian metamorphic rock when overlaying with geological map.

Figure 3.2 shows the gravity anomaly map. High gravity anomaly zones indicated by “A” have the located on northwestern and center part of gravity maps. These zones show Carboniferous sandstone, Permian limestone, Permo-Triassic volcanic rock, and Quaternary sediment when overlaying with geological map. Intermediate anomaly zones indicated by “B” have the NE-SW trend that is located on the center and southeastern of gravity anomaly maps. These zones show Quaternary sedimentary and Silurian-Devonian metamorphic rock when overlaying with geological map. The low gravity anomaly zone is located on eastern and southeastern part of gravity anomaly map indicated by “C” on.

These zones show Carboniferous sandstone, Silurian-Devonian metamorphic rock when overlaying with geological map.

However, high anomalies zone indicated by “A” on both of gravity and magnetic anomalies maps. These zones show Quaternary sediment when overlying with geological map. In general, the sedimentary unit should provide the low anomalies of both maps because of the low-density and low-magnetic susceptibility. Therefore, the forward modeling is produced across high anomaly zone on gravity anomalies map by AA' profile Figure 3.2.

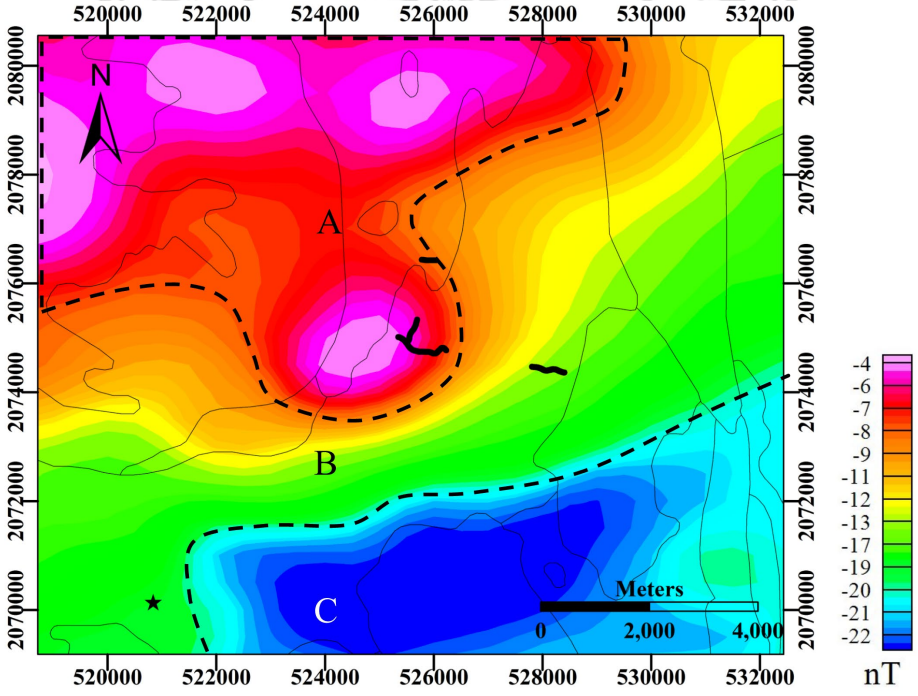

Figure 3.1 expresses high, intermediate, and low anomaly zones indicated by A, B, and C, respectively, on the RTP of residual magnetic map overlapped with boundary of geological units (Department of Mineral Resources, 1989).

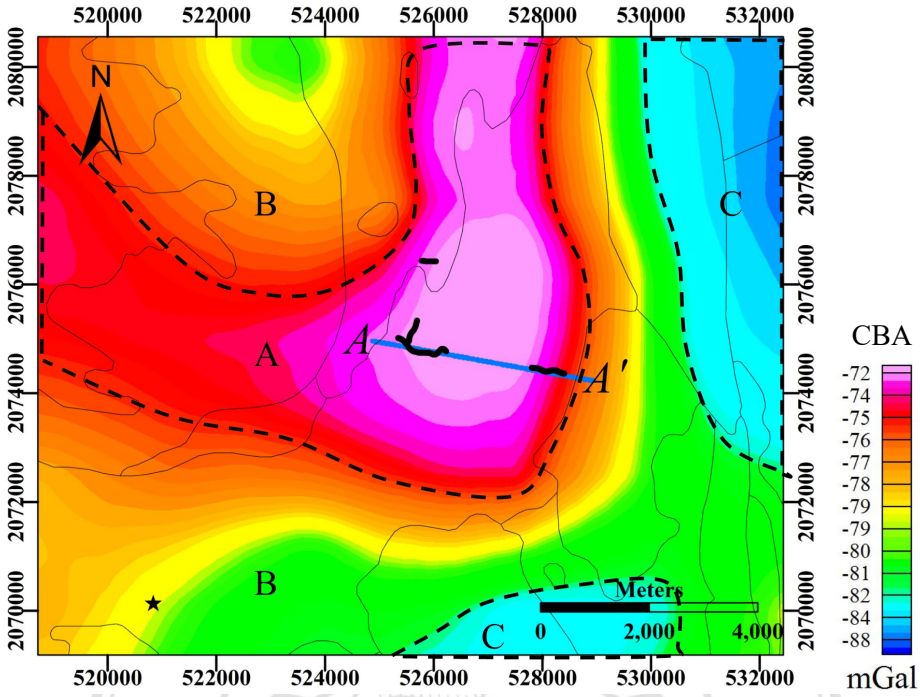

Figure 3.2 expresses high, intermediate, and low anomaly zones indicated by A, B, and C, respectively, on the ground gravity anomaly map overlapped with boundary of geological units (Department of Mineral Resources, 2015). Two-dimension forward modeling profile line AA' is crossed overlap two seismic reflection lines from west to east direction.

3.2. Wavenumber domain analysis of potential field data

The potential data are measured and considered as the discrete function in spatial domain (function of the position x and y). The discrete data point per unit distance is called as the sampling frequency. Frequently, the potential field data gridded in spatial domain are processed and analyzed in spatial frequency or wavenumber domain for convenient and qualitative interpretation.

3.2.1. Concept of wavenumber domain of analysis

The mathematic tool that transform data between spatial domain and frequency (wavenumber) domain is the 2D Fourier transform and defined by (Blakely, 1995):

$$F(k_x, k_y) = \int_{-\infty}^{\infty} \int_{-\infty}^{\infty} f(x,y) e^{i(k_x x + k_y y)}\, dxdy \qquad (3.1)$$

and its inverse Fourier transform is

$$f(k_x, k_y) = \frac{1}{4\pi^2} \int_{-\infty}^{\infty} \int_{-\infty}^{\infty} F(x,y) e^{i(k_x x + k_y y)}\, dk_x dk_y \qquad (3.2)$$

where $f(x,y)$ represents the input grid in spatial domain and $F(k_x, k_y)$ is the Fourier transform of $f(x,y)$. k_x and k_y are wavenumber components for function $F(k_x, k_y)$ measured in x and y directions. They relate with wavelength as $k_x = 2\pi/\lambda_x, k_y = 2\pi/\lambda_y$ which λ_x and λ_y are the apparent wavelength in x and y directions, respectively. Then, the relationship between wavenumber and wavelength of Fourier domain $F(k_x, k_y)$ is

$$k = \sqrt{k_x^2 + k_y^2} = \frac{2\pi}{\lambda} \qquad (3.3)$$

A Transformed grid $F(k_x, k_y)$ values, amplitude function, are complex numbers consist of real and imaginary part components and are the function of wavenumbers which have unit of cycles/ground-unit or general cycles/meter. Data in spatial domain have been sampling at even distance called grid cell size or grid spacing. Therefore, the transformed grid samples the Fourier function at even increments of 1/(grid size) with unit of cycle/ground-unit between 0 and Nyquist wavenumber (1/[2×cell size]).

The radially average power spectrum $E(k)$ is determined from the 2D complex Fourier amplitude spectrum. It is the average summation of the square complex Fourier amplitude function $F(k_x, k_y)$ along the same wavenumber k, the circle with radius k on the 2D Fourier domain. The plot between logarithm of that average versus wavenumber k is called the radially average power spectrum plot. Each point on graph in Figure 3.3 indicates the average of all point value lying on the circle with constant frequency or wavenumber k (Geosoft Inc., 2007). The Fourier transform converses the spatial domain into wavenumber domain up to Nyquist wavenumber. Hence, the radially average power spectrum is shown unto Nyquist wavenumber as well.

The subsurface structures could be obtained from the potential fields effect from their physical properties, density and magnetic susceptibility, distribution. The potential values are come from the superposition of the internal earth structure. There is fundamental relationship between the wavenumber and depth (Spector & Grant, 1970; Geosoft Inc.,

2007) that can be analyzed to separate the deep or shallow sources by depth estimating. The radially averaged power spectrum is a function of both radial frequency and radially azimuth direction. Finally, the average source depth is obtained from the slope of linear decay curve. Noticeable the changes in dominant slope indicate the presence of sources at more than one characteristic depth so each linear gradient must be analyzed separately. The gradient portion of linear curve represents the depth of subtle bodies. Then the radially averaged power spectrum analysis is used as a tool for depth estimation (Geosoft Inc., 2007). From graph in Figure 3.3, the steepest gradient in the low wavenumber part indicates deep source (regional) component, while the gently slope in the high wavenumber part represents a shallow source (residual) component. The relationship between the logarithm of radially average power spectrum $E(k)$ and the statistic depth can be expressed as (Geosoft Inc., 2007):

$$\log E(k) = -4\pi hk \tag{3.4}$$

$$h = -\frac{1}{4\pi}(slope) \tag{3.5}$$

where h is the depth in kilo-ground unit (kilometer) and k is wavenumber in cycles per kilo-grounds unit (1/kilometer).

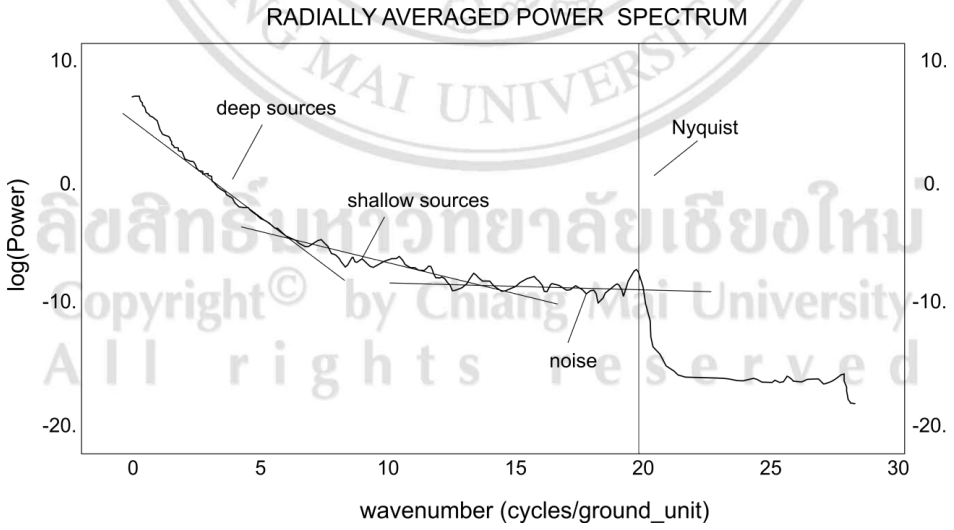

Figure 3.3 presents the radially averaged power spectrum of sample gravity map and geological source depth approximation, noise and Nyquist wavenumber (Geosoft Inc., 2007).

3.2.2. Depth estimation of potential filed data

The upper diagram of Figure 3.4a illustrates the logarithm radially averaged power spectrum of aeromagnetic map against wavenumber (1/km) resulted from the Fourier transform of the RTP map in Figure 3.1. The lower diagram shows estimation of depth that relates to the slope of upper diagram in log scale (Figure 3.4b). According to Figure 3.4a, the steepest slope "1" corresponding to wavenumber between 0 and 0.15 (1/km) represents the deep magnetic source with depth about 1.1 to 2.3 kilometers. The moderate slope "2" corresponding to wavenumber between 0.5 and 1.1 represents the shallower magnetic source with depth about 0.5 to 1.1 kilometers. The gentle slope "3" corresponding to wavenumber greater than 0.8 represents the near surface magnetic source with depth about 0-500 meter.

The upper diagram of Figure 3.5a illustrates the logarithm radially averaged power spectrum of gravity data against wavenumber (1/km). The lower diagram shows estimation of depth that relates to the slope of upper diagram in log scale (Figure 3.5b). According to Figure 3.5a, the steep slope "1" corresponding to wavenumber between 0 and 0.17 (1/km) represents deep magnetic source with depth about 1.8 to 2.5 kilometers, the steep slope "2" corresponding to wavenumber between 0.17 and 0.8 represents shallower magnetic source with depth about 0.25 to 1 kilometers. The gentle slope "3" corresponding to wavenumber greater than 0.8 represents near surface magnetic source with depth approximate near-surface to 0-1000 meter.

According to the radially average power spectrum, the steep slope "1 and 2" are the results from basement which is 1-2 km depth. The gentle slope "3" from gravity and magnetic anomaly map provided from information near-surface source which is basalt layer, depth of the layer varies between 500-1000 m. The depth that derived from this method is used for creating initial forward modeling for gravity modeling later.

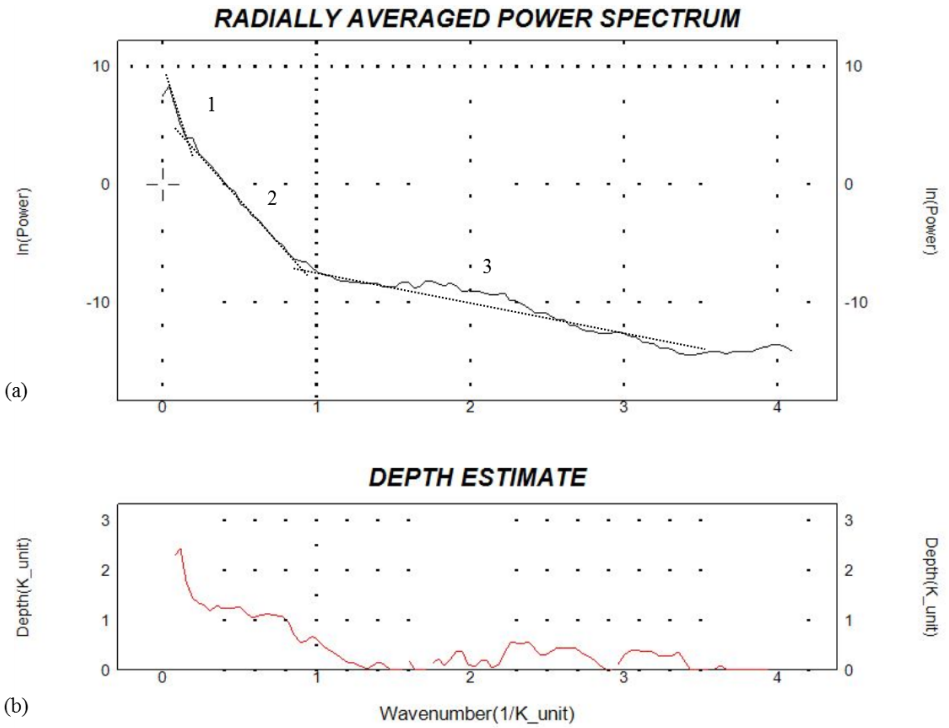

Figure 3.4 shows the radially average power spectrum of the magnetic map in Figure 3.1

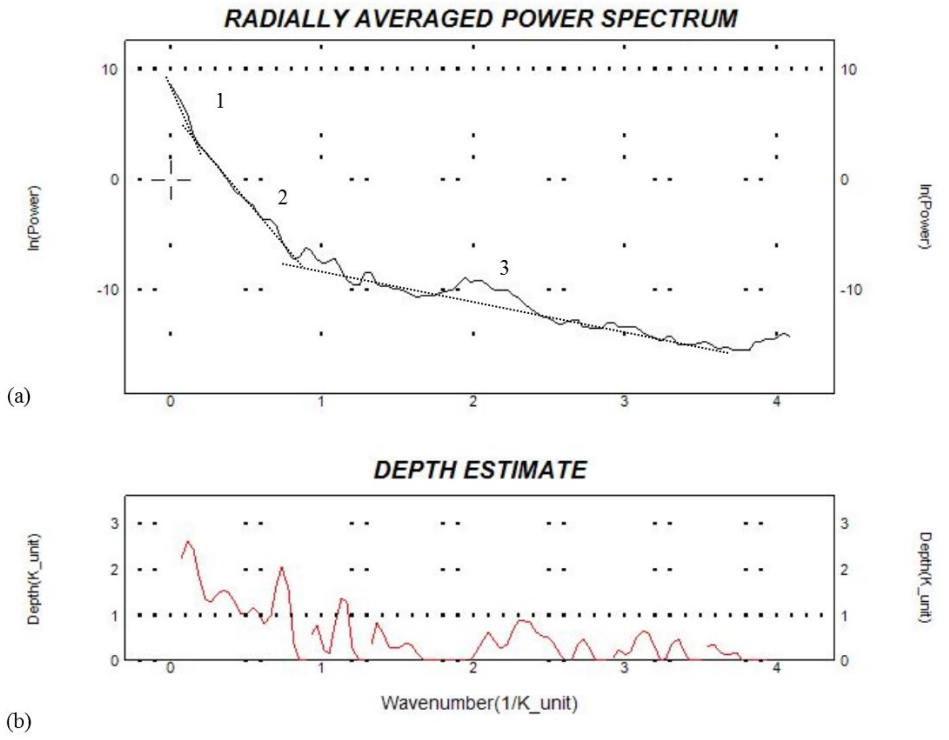

Figure 3.5 shows the radially average power spectrum of the complete Bouguer map in Figure 3.2.

3.3. 2D Forward modeling of gravity data

Seismic data interpretation from Chapter 2 and the estimated depth information from radially average power spectrum of gravity and magnetic anomalies are utilized to constrain the construction of subsurface model. This topic explains the 2D forward modeling of gravity data along the profile AA' which overlapping with seismic reflection Line MO-1 in the west and Line MO-4 in the east.

3.3.1. Concept of 2D forward modeling

The objective of the forward calculation in geophysical method is to acquire the geophysics data response by assigned earth's physical properties with earth's geometry, Blakely (1996). The two-dimension modeling are constructed by using GM-SYS Geosoft Oasis Montaj software (Geosoft Inc., 2007). GM-SYS allows the simulation calculations of the potential field effects of a cross-section consisting of an assumed geologic with different densities base on variation of geology setting. The GM-SYS evaluates the gravity effects at specified points along selected profile with an assumed geologic cross section and compares these calculated values to the observed values. The assumed model is then modified until an acceptable agreement is reached between calculated and observed values. The mentions on this paragraph can be explained on Figure 3.6 which shows a flowchart diagram for forward modeling calculation.

3.3.2. 2D gravity model

This topic focus on gravity data responses base on density. Gravity anomalies map (Figure 3.2) over the Mae On basin was modeled by two dimensional interactive forward modeling using GM-SYS. The two-dimension forward modeling profile AA' is crossed overlap the two reflection seismic lines (Figure 3.2) which used as the initial model to constrain shallow geometry depth. The seismic profiles could only provide the information to constrain until depth of about 180 m because the seismic energy could not penetrate through the deeper zone. Therefore, the modeling will be concentrated on the near-surface geometry. The density is the main parameter to construct a Pseudo-geological model, therefore, the density values are estimated from available information. The initial density of rock in this study are derived from gravity survey in the adjacent

area Chiang Mai Basin, Wattananikorn *et al.* (1995), internal reported from Geophysical Research laboratory, Chiang Mai University (Saengthip, 2016), and geophysics textbook (Telford *et al*., 1990) as shown in Table 3.1.

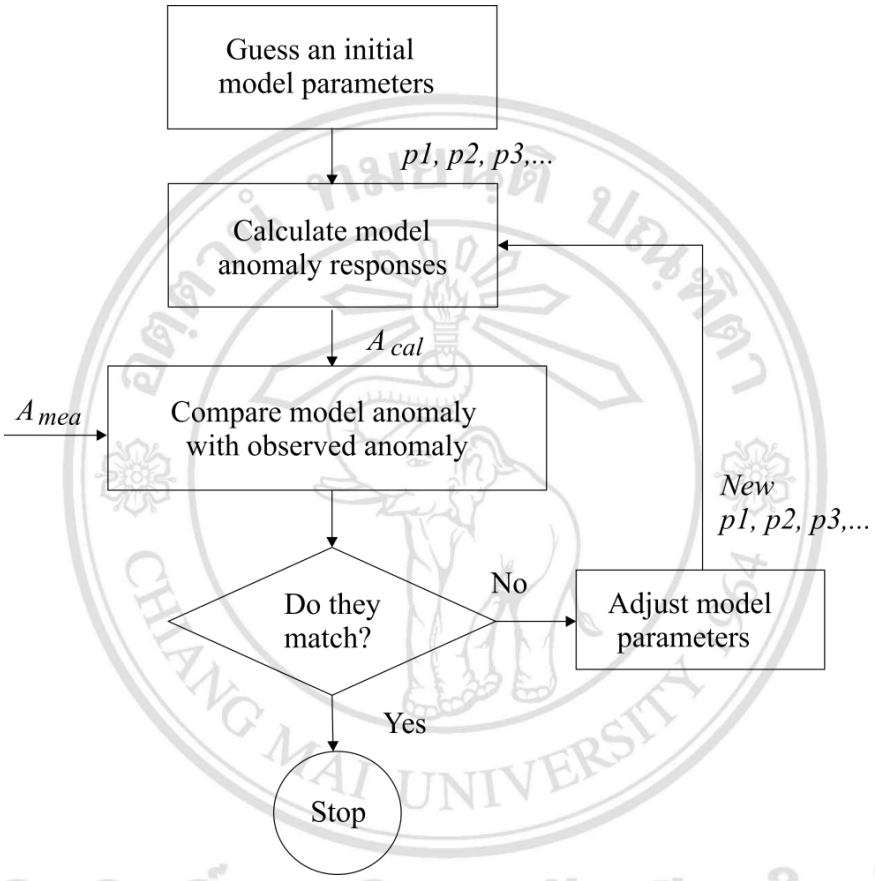

Figure 3.6 displays a flowchart diagram for forward modeling. A_{mea} is measured anomaly while A_{cal} is calculated anomaly (modified from Blakely, 1995).

The seismic cross-sections and geological map are used for initiating and to constrain the pseudo-geological model. According to the geological map on Chapter 1, the western side of the study area contacts with Carboniferous sandstone, while the western side is contacted with Silurian-Devonian metamorphic rocks. Wattananikorn *et al.* (1995) defined the densities of Paleozoic and older rocks in Chiang Mai Basin as 2.60 g/cm^3. Then, the density of Carboniferous sandstone rocks and Silurian-Devonian metamorphic rocks for this study are defined as 2.60 g/cm^3 as well.

Table 3.1 lists densities for various kind of rock (Modified from Telford *et al*., 1990)

Rock type	Density (g/cm^3)	
	Range	Average
Sand	1.70-2.30	2.00
Sandstone	1.61-2.76	2.35
Shale	1.77-3.20	2.40
Limestone	1.93-2.90	2.55
Sedimentary rock (average)		2.50
Basalt	2.70-3.30	2.99
Granite	2.50-2.81	2.64
Gabbro	2.70-3.50	2.64
Basic igneous (average)		2.79
Slate	2.70-2.90	2.79
Gneiss	2.59-3.00	2.80
Metamorphic rock (average)		2.74

The outcrop zone of basalt rock was found in the center of the study area. From the interpretation of seismic cross-sections in Chapter 2, the basalt layer is overlying by weathering layer. The bottom of weathering and basalt layers have the depth approximately about 5-10 and 30-40 m from surface, respectively. The density of sediment layer is estimated from Wattananikorn, et al., 1995. They defined that the topmost layer density was about 2.0 g/cm^3. The volcanic rock density is estimated from the internal report (Saengthip, 2016) for this study, the average basalt density equal to 2.95 g/cm^3 was used.

The part underneath basalt layer is presumed as many of the pyroclastic layers base on four reasons. First, those layers are contacted with basalt layer, therefore the environment when they accumulate should be similar. Second, the origin of pyroclastic deposits as a horizontal layer in each of event, the seismic reflection profiles can confirm by horizontal reflectors (Figures 2.30, 2.31, 2.32, and 2.33). Third, there is high resistivity layer which underlying basaltic layer in the electrical resistivity profile (Figure 2.35). It is consequence related to volcanic rock, however, this layer has lower resistivity value than that of basaltic layer. Last, the depth analysis by using the radially average power

spectrum from potential field confirms that there is the volcanic rock at about 500-1000 m depth.

The velocity estimated from seismic reflection method indicates that the pyroclastic layer (MU1) which underlying basaltic layer (UU) has lower velocity and then the MU2 and LU layers have the velocity increased with depth. According to the reasons, the densities of pyroclastic layers are identified base on relationship of velocity value. The first pyroclastic layer (MU1) is considered an average density that equal to 2.75 g/cm^3. The second and third pyroclastic layers (MU2 and LU), considered an average density that equal to 2.80 and 2.85 g/cm^3, respectively.

The initial forward modeling is constrained by available information, the depth estimates from the radially average power spectrum constrains the deeper zone which indicates the boundary of the volcanic source about 750 m depth. Whereas, the results from resistivity, MASW, and seismic refraction methods constrain the shallow zone and first basalt layer. Moreover, the horizontal layers, MU1, MU2, and LU underneath basalt layer are confirmed by seismic reflection profile.

For forward modeling of line AA', the independent densities as mention above were input as initial parameters and tested. The parameter and model adjustments were done by the best fitted between calculated and observed of the gravity response from the pseudo-geological model. Table 3.2 shows the summation of densities in forward modeling. The final pseudo-geological model resulted from forward modeling of line AA' is displayed in Figure 3.7.

Table 3.2 shows the summation of density values in the final pseudo-geological model.

Seismic units	Lithological units	Densities (g/cm^3)	Reference sources
UU	Top soil	2.0	Wattananikorn *et al.* (1995)
	Basalt	2.95	Saengthip (2016)
MU1	Pyroclastic1	2.75	Telford *et al*. (1990) and seismic reflection
MU2	Pyroclastic 2	2.8	
LU	Pyroclastic 3	2.85	

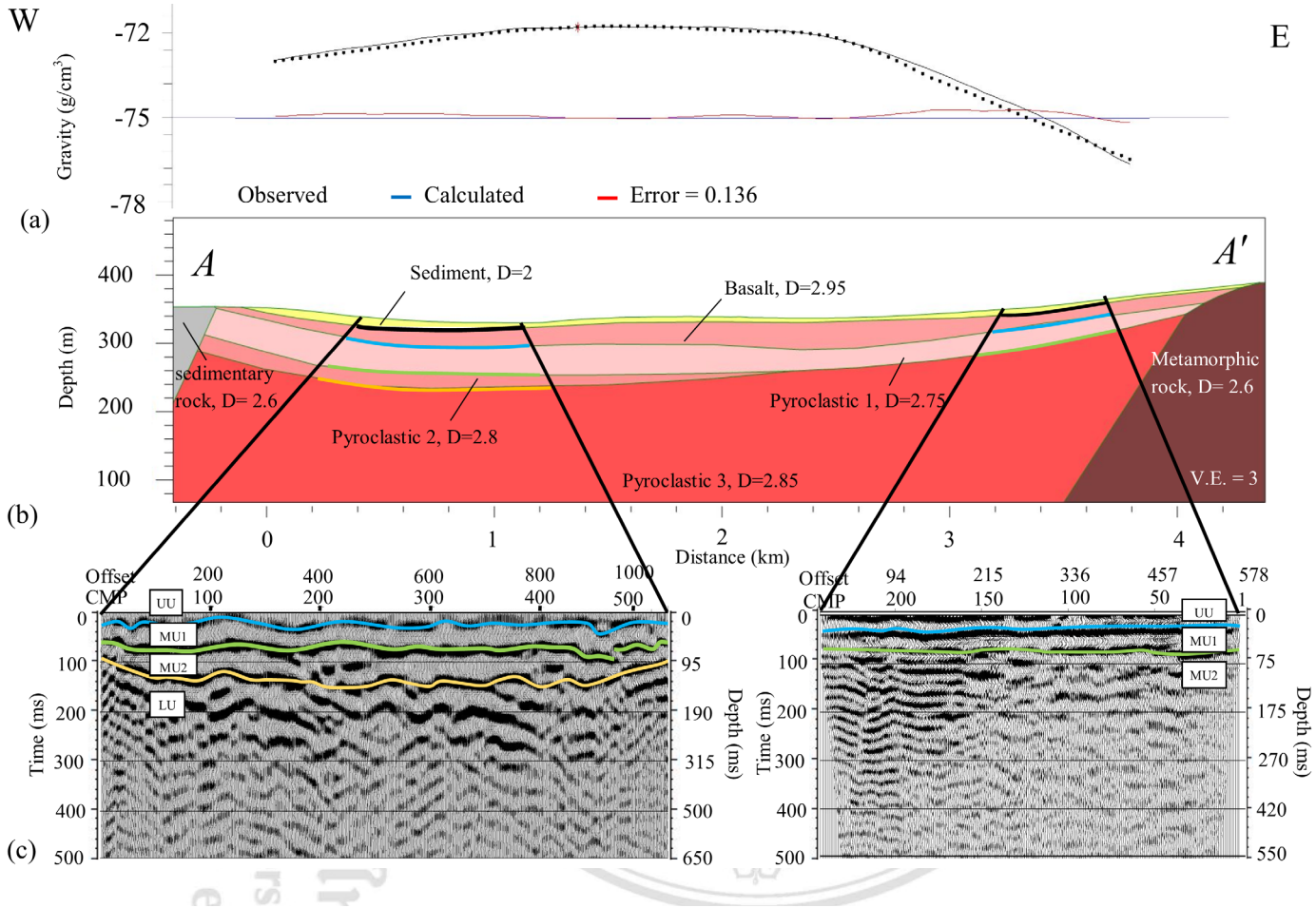

Figure 3.7 shows forward modeling form profile AA' (a) the observed and calculated gravity anomalies with density in g/cm^3 (D), (b) the final pseudo-geologic model constrained by (c) seismic cross-sections from Line MO-1 (left) and MO-4 (right).